Open-Circuit Fault Detection in Stranded PMSM Windings Using Embedded FBG Thermal Sensors

Anees Mohammed, Juan I. Melecio, and Siniša Djurović, *Member, IEEE*

***Abstract*— Detection of winding faults in permanent magnet synchronous machines (PMSMs) with stranded winding designs remains a challenging task for conventional diagnostic techniques. This paper proposes a new sensing approach to this problem by investigating the application of dedicated electrically non-conductive and electromagnetic interference immune fiber Bragg grating (FBG) temperature sensors embedded in PMSM windings to enable winding open-circuit fault diagnosis based on observing the fault thermal signature. The final element analysis thermal and electromagnetic models of the examined practical PMSM design are first developed and used to enable the understanding of open-circuit winding fault-induced signature that can be used for effective diagnostic purposes, indicating *in situ* thermal excitation as an optimal diagnostic measurand. A purpose build test rig with an inverter-driven commercial PMSM instrumented with *in situ* FBG sensors monitoring phase winding hot spots is then used to evaluate the efficacy of the proposed diagnostic scheme. It is shown that unambiguous diagnosis and severity trending of winding open-circuit faults is enabled by the use of *in situ* FBG sensors. A comparison with conventional fault diagnostic technique utilizing current signal sensing and analysis is also reported, indicating the considerable advantages of the proposed monitoring scheme employing FBG sensors.**

***Index Terms*— Fiber Bragg grating sensors (FBG), embedded thermal monitoring, open circuit fault, PM machines, windings.**

I. Introduction

PERMANENT Magnet Synchronous Machines (PMSMs) are key elements of a number of contemporary industrial systems, ranging from application as preferred propulsion motor choice in modern electric vehicles (EVs) to being enabling components of military, medical, factory automation, aerospace and wind energy systems [1], [2]. A large proportion of PMSM applications in these areas is safety- and/or operationally-critical. The capability of reliable and timely diagnosis of PMSMs faults has thus become an important requirement for effective utilization of these systems [1]–[3].

Manuscript received December 12, 2018; revised January 14, 2019; accepted January 15, 2019. Date of publication January 31, 2019; date of current version April 5, 2019. This work was supported by the U.K. Engineering and Physical Sciences Research Council (EPSRC) through HOME-Offshore: Holistic Operation and Maintenance for Energy from Offshore Wind Farms Consortium under Grant EP/P009743/1. The associate editor coordinating the review of this paper and approving it for publication was Dr. Carlos Marques. *(Corresponding author: Siniša Djurović.)*

The authors are with the School of Electrical and Electronic Engineering, University of Manchester, Manchester M13 9PL, U.K. (e-mail: anees.mohammed@manchester.ac.uk; ignacio.melecio@manchester.ac.uk; sinisa.durovic@manchester.ac.uk).

Digital Object Identifier 10.1109/JSEN.2019.2894097

PMSMs faults are generally classified as: electrical (stator), and magnetic and mechanical faults [4]. The available surveys indicate stator winding faults as one of most commonly occurring in electrical machines, including PMSMs [5]. These faults are caused by progressive degradation of conductor insulation. Their root cause is largely in the combination of operating thermal, mechanical and electrical stress, and environmental factors related to the application in which these machines operate [5], [6]. Winding faults are generally defined as short circuit (SC) or open circuit (OC) faults; the latter can result from a SC fault but can also be initiated due to improper connection or excessive vibration [7], [8].

PMSMs stator windings are generally configured with single or with multiple parallel strands [9]. In a single stranded design OC faults generally lead to electric and magnetic asymmetries, resulting in apparent phase currents unbalance and vibrations [10], [11]. In a stranded winding design however, the effects of OC fault can be inherently mitigated as the required current is allowed to flow in the remaining healthy parallel strands of the faulted phase, thereby providing a measure of fault tolerance [12]; this can significantly complicate OC fault diagnosis based on conventional electrical or mechanical signal based diagnostic indices. In this winding design, any existing OC fault in the parallel strands may therefore result in an increase of the heat loss produced in the faulted phase compared to normal operation. This fault induced heat can lead to degradation of the neighboring healthy strands integrity and increase the risk of rotor PMs demagnetization [8], [13]. Enabling effective detection of OC faults in multiple parallel strand winding design is therefore important to prevent further, potentially disastrous, machine damage and enable predictive maintenance strategies. This is particularly pertinent in PMSM machinery where due to the presence of permanent magnets on the rotor, electrical faults must be rapidly detected and appropriate mitigating measures put in place to prevent catastrophic machine failure.

PMSM winding fault diagnosis has steadily been gaining increased attention [2], [14]–[17]. The reported techniques largely rely on noninvasive electric and electromagnetic signals monitoring methods that have been widely applied in induction machines, e.g. spectral examination for fault signature definition in signals such as current, voltage or flux. When winding fault diagnosis in PMSM machinery is concerned these have shown limitations due to the challenge of identifying reliable and consistent fault spectral signature [2]. To overcome this, application of advanced artificial

intelligence methods, such as neural networks, was proposed; these can however suffer from diagnostic unreliability and require large data sets for training [18].

Thermal monitoring, fundamental for electrical machine protection and health monitoring [19], could present a promising alternative to examined PMSM winding fault techniques. However, advanced on-line thermal monitoring use for stator winding fault diagnosis has not been widely investigated [20], [21]. This is due to operational limitations of conventional thermal sensing techniques used in electric machines, in timely, reliably and effectively accessing and measuring the fault induced thermal signature (i.e. localized hot-spots) within the winding structure. Resistance based thermal estimation techniques, while non-invasive, only provide average winding temperature and are thus ineffective for monitoring hot spots such as those induced by winding faults [22]. Thermal imaging was shown to carry some potential for winding fault diagnosis [23], however this is not amenable to practical application as it is based on monitoring thermal variation of machine frame surface and thus cannot provide timely diagnosis of fault. Winding embedded thermal sensing techniques, based on application of thermocouple (TC) or resistance temperature detector (RTD) sensors could in principle provide information on localized winding temperature. However, the use of these sensors for enabling distributed sensing is limited by the required number of sensing points and their installation complexity caused by sensor bulk and number of connections required; in addition, their inherently conductive structure and sensitivity to electromagnetic interference largely limit their embedment in direct contact with winding conductors; they are consequently predominantly utilized for thermal monitoring in end winding sections where their bulk and wiring can be better accommodated [19], [21].

Fiber Bragg gratings (FBGs) are a sensing technique utilizing microstructures inscribed in optical fibers and present an attractive prospect for in-situ component embedded sensing application in electrical machines. FBG use in machine sensing applications has started to gain increased interest in recent years [24]–[28]. These optical fiber sensors have inherent advantages over existing conventional thermal sensors for winding thermal monitoring, and in particular under electric fault conditions: they are electrically passive, light weight, small in size, fully electromagnetic interference (EMI) immune and can be multiplexed, allowing for winding in-situ thermal sensing capability and facilitating distributed embedded sensing [24]–[28]. Author's previous work has examined FBG sensing design and application for low voltage winding interior thermal monitoring [24], [28], [29].

The use of FBG thermal sensors for in-situ monitoring of internal thermal excitation in low voltage inverter driven PMSM machines has not been researched. FBG sensing technology has considerable potential to provide effective winding fault diagnostic solutions for widely used PMSM applications. This study therefore reports an investigation of OC fault thermal signature monitoring for diagnostic purposes in parallel stranded winding PMSM designs utilizing the author's previously reported in-situ FBG sensor design [28]. To this end a purpose designed laboratory test rig was built containing an inverter driven 5.5 kW stranded winding PMSM that was rewound to enable practical OC fault emulation and instrumented with winding embedded FBG sensors in addition to a conventional current sensor suite. The diagnostic signature of OC faults in thermal and electrical PMSM signals was first analyzed by performing electro-magnetic and thermal finite element analysis (FEA) models simulations to facilitate understanding of attainable diagnostic indices in practically sensed electrical and thermal signals. A series of experimental tests was then carried out to investigate the in-situ thermal FBG sensor's diagnostic performance under OC faults. In-situ fault thermal signature trending was also assessed for a range of OC fault severities and operating load conditions to evaluate its consistency and diagnostic potential. Finally, the FBG diagnostic performance was compared with that of current signal analysis conventionally used in electric machines fault diagnosis.

TABLE I
PMSM SPECIFICATIONS

PMSM Data	Type: HPS1141500
Rated Power / Voltage / Current	5.5 kW / 400 V / 11.5A
Rated speed/ Frequency	1500 rpm/ 75 Hz
Pole number/ Rotor configuration	6 / Surface mounted magnet
Slot number stator	39
Insulation class / Temperature rise class	F / B
Duty cycle type rating	S1
Design standard	IEC 60034

To facilitate the understanding of sensing requirements for effective OC fault signature recognition, this section undertakes a multi-physical FEA model analysis of OC fault electrical and thermal characteristics of a commercial stranded winding PMSM design examined in this work. This allows the possible and optimal measurands associated with OC fault presence to be identified and the requirements for their sensing and monitoring to be defined. To this end, an electromagnetic and a thermal FEA model of the examined 5.5 kW test PMSM (specification shown in Table I) were developed using Cedrat Flux2D and Motor-CAD commercial FEA software packages. Steady-state operation in the generating range with the stator windings connected to a resistive load was simulated for the purpose of this study, to enable a clear identification and characterization of fault effects and signatures. Fig. 1 shows the stator phase winding design of the test PMSM: the healthy winding, Fig. 1a, is seen to consist of six parallel strands, each containing six coils, where each coil has 23 turns; a diagram of a three strand OC fault in this winding is presented in Fig. 1.b for illustrative purposes. The developed test PMSM electromagnetic and thermal models were used to perform a series of simulations of respective features of its behavior in healthy conditions and under OC fault severities ranging from one to four strand open circuits in phase A at rated conditions (1500 rpm and 100% load).

A. Electromagnetic Model Study

Electromagnetic FEA model stator current predictions for simulated healthy and OC fault conditions are shown in Fig. 2.

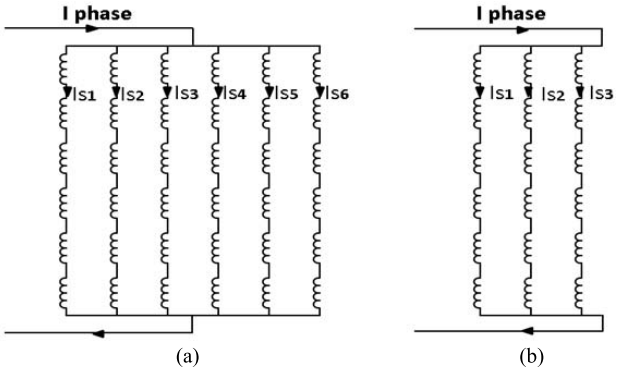

Fig. 1. (a) Healthy phase winding and (b) a three strand OC fault.

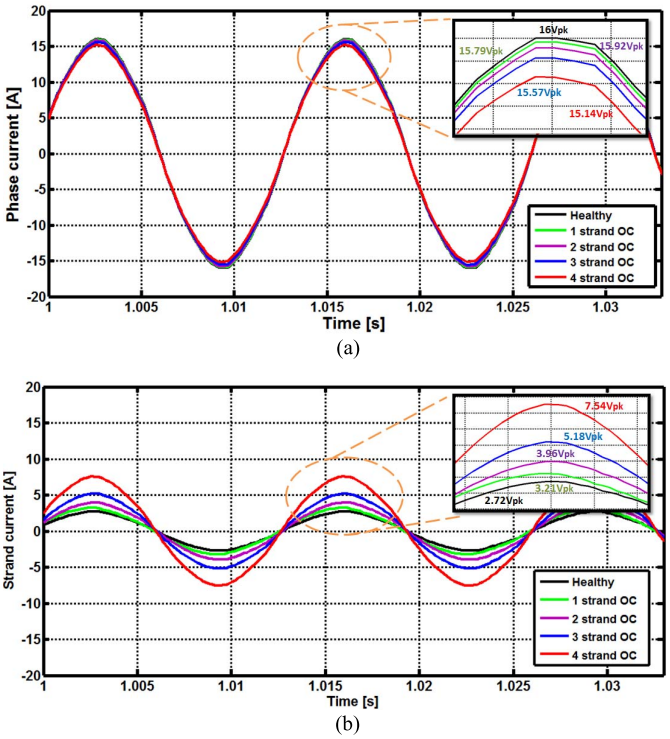

Fig. 2. 2D flux model results comparison under OC fault conditions. (a) Phase A currents. (b) Strand currents.

The superimposed results of the phase current predicted for the healthy and all the examined OC fault cases (i.e. 1, 2, 3 and 4 strand OC) are shown in Fig. 2a, while the corresponding model results for healthy strand current are shown in Fig. 2b, respectively. The phase current is seen to exhibit a slight reduction with fault presence and severity increase; this is the result of phase impedance increase with the reduction in the number of parallel active strands. The load impedance coupled to the system is driving the power drawn from the machine; the phase current level therefore remains close to the nominal value, as further illustrated in the inset detailed view in Fig. 2a. The predicted rms current value of the healthy phase A current is ≈11.30 A at 100% load and with a 4 strands OC fault, is calculated to be ≈10.70 A, presenting a slight variation of ≈5%. However, regarding current flow and magnitude in the

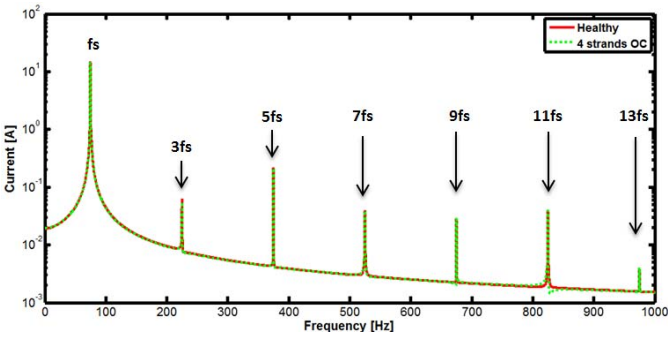

Fig. 3. FFT spectral results of phase A current.

winding strands, the phase current is divided across the active parallel strands of the winding: combined with the observed low level variation in phase current with OC fault presence this suggests that the strand current rms value can be expected to manifest a considerable increase with OC fault severity. The predicted rms current value in case of 1 strand OC is seen to increase from ≈1.88 A at no fault conditions to ≈2.26 A in the presence of fault. The strand current rms value is seen to increase further with OC fault severity increase: with four stands opened, it is predicted to reach ≈5.35 A, which is a ≈285% increase on the healthy value.

From the PMSM condition monitoring (CM) for winding fault diagnosis point of view, monitoring the time domain phase current does not enable diagnosis of OC faults as there is no significant change in its magnitude between healthy and faulty conditions; thus, the standard motor protection systems are not expected to react to this type of fault. Individual strand current sensing and monitoring on the other hand is not practically attainable in a stranded winding configuration examined here. A common diagnostic approach for ac machinery is based on examining fault specific spectral changes (i.e. signature) in the current signal – the MCSA analysis method [2]. MCSA was therefore applied on the FEA model predicted phase current in a Fast Fourier Transform (FFT) 2^{15} data point spectrum. For illustration, the 0-1000Hz current spectra obtained for a healthy machine and a 4 strand OC fault are shown in Fig. 3. As can be seen, the spectral harmonic content under fault remains almost identical compared to that in the healthy condition; the harmonic spectrum contains the fundamental frequency, fs, and its odd harmonics (e.g. 3fs, 5fs, 7fs etc.), as is generally expected in a PMSM; these originate from the spatial distribution of the air-gap flux density produced by the rotor permanent magnets that is in principle not considerably affected by presence of a strand OC fault [1], [30], [31]. The obtained results show that there is no clear OC fault spectral indicator in the current spectrum. This illustrates the challenge of detecting this fault type in PMSMs using the current signature monitoring method.

B. Thermal Model Study

The simulated current results from the electromagnetic FEA model were used in the thermal FEA model to simulate the thermal effects of OC faults in PMSM stator windings.

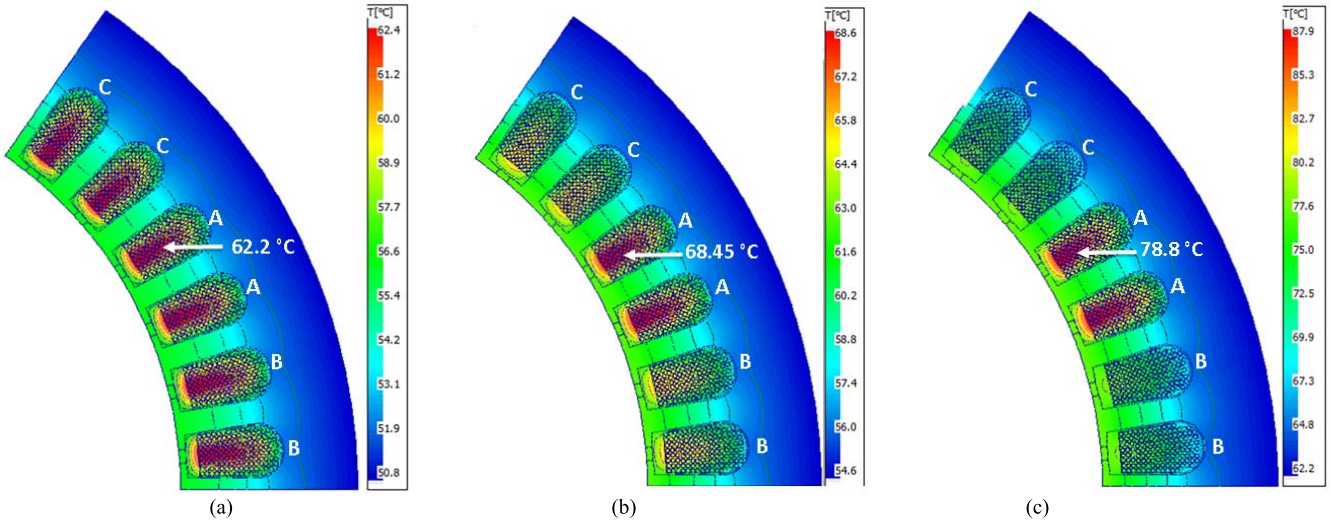

Fig. 4. Simulated OC fault thermal results represented as temperature gradients: (a) full load/healthy condition, (b) full load with 2 parallel strands opened, and c) full load with 4 parallel strands opened.

The current data was used to calculate the variation in the winding losses due to OC fault for each examined fault severity. The developed thermal model is a 2D model of the stator windings slot section. Due to the requirements of conventional heat transfer/aerodynamic characteristics, which are challenging to model in the used commercial software end-winding analysis is not included in the developed model. In general, due to end winding thermal averaging effects, the thermal effects observed in the slot section with fault would be expected to be less pronounced in the end winding section [24].

Fig. 4 shows the 2D-FE thermal results of a stator section under healthy and faulty conditions (shown for one pole pitch of the stator for illustration purposes). The examined stator section comprises six slots, two per phase winding (i.e. top two belong to phase C, mid two to phase A and bottom two to phase B). The simulated thermal results obtained for healthy winding (see Fig. 4a), 2 strand OC (see Fig. 4b) and 4 strand OC fault (see Fig. 4c) are presented to illustrate the nature of fault induced thermal effects.

The predicted data show the fault induced thermal hot spots in the faulty phase (phase A, mid two slots) and the hot spot temperature rise with the fault severity. In healthy conditions, the windings manifest an almost identical temperature in the slots for all phases with a hot spot of ≈62.2 °C in the slot center. In OC fault presence, the temperature gradient and hot spots are redistributed; in the 2 strand OC case, phase A slots temperature increases and their hot spot temperature rises to ≈68.49 °C. In the case of 4 strand OC the hot spot increases to ≈87.8 °C. These results show a hot spot temperature rise in the faulty phase of up to ≈25.6 °C compared with that of a healthy winding. The remaining phases also show a slight temperature rise due to the heat transfer from the faulty coil through the stator core (i.e. teeth and yoke).

Despite the number of the phase turns carrying current within the slot reducing with increase in the number of opened strands (i.e. OC fault severity increase), the total stator slot heat loss shows an increase. The increase and redistribution of winding temperature under fault conditions largely results from the increase of associated heat losses (I^2R). This is a result of the faulty phase current rebalancing between the remaining healthy strands, as observed in study in section II.B. Table II shows the simulated values of the phase and strand current, and heat losses and hotspot temperature for a faulty phase A slot. It can be seen that the heat losses are increased in the slot from ≈3.9 W in healthy conditions to ≈11.8 W with 4 strands OC. The obtained results clearly indicate a thermal signature magnitude rise induced due to the presence of OC fault.

TABLE II
HEAT LOSS CALCULATIONS

condition	Phase current (A)	Strand current (A)	R/conductor /slot length (Ω)	Active turns (turns)	Loss per slot (W)	Loss Increase (%)	Hotspot (°C)	Hotspot rise (°C)
healthy	11.30	1.88	0.009	138	4.39	0.00	62.2	0
1 strand	11.26	2.26	0.009	115	5.29	20.43	65.2	3
2 strands	11.17	2.80	0.009	92	6.49	47.88	68.5	6.3
3 strands	10.99	3.67	0.009	69	8.36	90.54	77.6	15.4
4 strands	10.70	5.35	0.009	46	11.85	169.94	87.8	25.6

C. Sensing Requirements for OC Fault Diagnosis

The reported studies highlight the limitations of relying on electrical signal (e.g. current) sensing to achieve OC fault diagnosis, as fault induced changes in these are challenging to observe and interpret reliably. In contrast, the thermal study indicates that consistent localized thermal excitation resulting from OC fault presence in the stranded winding enables the use of thermal excitation monitoring for OC fault diagnosis, if this excitation can be properly sensed. An appropriate thermal sensing system design that enables effective monitoring of in-situ thermal signature in targeted winding positions (e.g. in the slot section thermal hot spot position) could therefore be key to enabling effective detection of OC winding faults in PMSMs with stranded windings. FBG thermal sensing technology presents a promising solution for

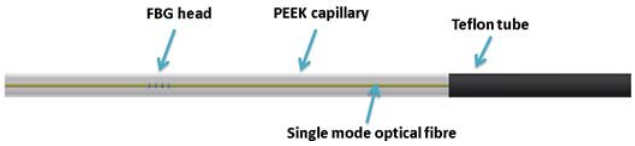

Fig. 5. In-situ FBG temperature sensor design.

this type of application and its implementation for this purpose is examined in the following sections.

II. In-Situ FBG Thermal Sensing System

A. FBG Sensing Principles

FBGs are the periodic gratings on the optical fiber core that result in a periodic modulation of its reflective index when exposed to an interference pattern of laser light [28]. The wavelengths reflected by the FBG structure will alter with the variation in the strain and/or temperature it and thermal excitation sensitive element. With an appropriate design, this phenomenon enables the grated fiber to be utilized as a mechanical or thermal sensor. The reflected wavelength variation due to temperature change can be expressed in terms of the fiber thermal characteristics as [32]:

$$\Delta\lambda_B = \lambda_B(\alpha + \xi)\Delta T \tag{1}$$

where: α is the fiber thermal expansion coefficient ($\approx 0.55 \times 10^{-6}/°C$) and ξ is the fiber thermo-optic coefficient ($\approx 6 - 9 \times 10^{-6}/°C$). Theoretically, for a standard bare FBG with the Bragg wavelength of 1550 nm operating at ambient temperature, the thermal sensitivity can be evaluated to be $\approx 10 - 14$ pm/°C [32].

B. Examined FBG Sensor Design

The in-situ FBG temperature sensors used in this work builds on authors previous research and is designed to be small in size, has dielectric properties and thus retain FBG inherent EMI immunity, and withstand temperatures up to ≈250 °C [24], [28]. These features are important requirements for enabling effective thermal sensing in the PMSM winding, in direct proximity to the random wound coil thermal hot spot where the thermal signature of OC fault is exhibited and can be monitored, as detailed in section II. In this design, the FBG is packaged in a polyetheretherketone (PEEK) capillary to enable exclusive thermal measurement and provide mechanical protection to the fragile sensing fiber embedded within the winding structure [28]. The sensor architecture is illustrated in Fig. 5, it consists of a single 5mm long FBG head imprinted in a polyimide coated fiber with a bandwidth of ≈0.374 nm and reflectivity of ≈88%. The fiber section containing the FBG head is loosely packaged within the PEEK capillary, while the remainder of the optic cable is tubed in Teflon for protective purposes. The final diameter of the sensing element with packaging is ≈0.8 mm. The FBG temperature sensors used in this study were thermally calibrated in an industrial thermal chamber following the procedure described in [24] and [28]. The FBGs' temperature sensitivity

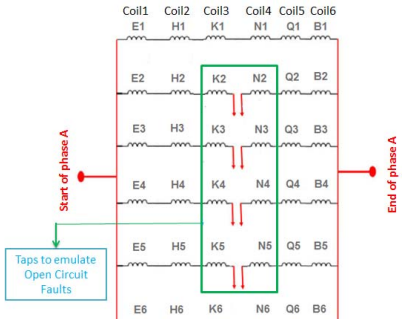

Fig. 6. Phase A winding diagram (for OC faults emulation).

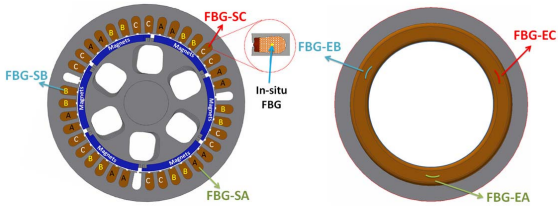

Fig. 7. Test motor thermal sensor positions: (a) FBG sensor locations in slot sections and (b) FBG sensor locations in front end winding.

coefficients average calculated from the slope of the calibration test data linear fits is ≈10.87 pm/°C, which matches the general theoretical calculated temperature sensitivity range of a bare FBG stated in section II.A

III. Experimental Test-Rig Description

A. PMSM Winding In-Situ FBG Thermal Sensors Network

The proposed stator winding OC fault on-line diagnostic technique based on in-situ thermal signature sensing was realized by installing a number of FBG sensing probes into the commercial PMSM design detailed in section II. The stator was rewound to enable sensors installation in targeted positions and experimental emulation of strand OC faults assumed to occur in phase A in this study. The test motor phase windings consist of 6 series connected coils, each with 6 parallel strands of 23.5AWG enameled copper wire; in the rewind process phase A winding was modified to allow emulation of OC faults involving 1, 2, 3 or 4 strands by tapping specific winding points, as shown in Fig. 6.

Fig. 7 illustrates the target locations within the winding in which FBG sensors were embedded. Three probes were installed and distributed in three stator winding slot sections, one per phase winding: one each in a slot containing a healthy phase coil (FBG-SB and FBG-SC for healthy phases B and C, respectively) and the remaining sensor in the slot containing a coil of the faulted phase A (FBG-SA), as shown in Fig. 7a. The sensing head of each FBG probe was placed between the copper conductors in the slot section cross-sectional center point at core axial length mid-point during the rewind process, as illustrated in Fig. 8. In addition to the FBGs embedded in the slot section, three FBG sensors were embedded in the end-winding section in thermal detector locations specified

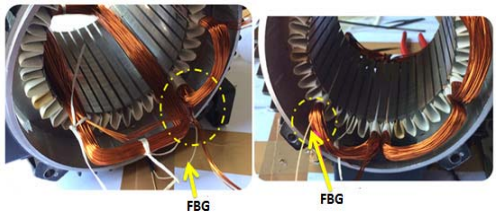

Fig. 8. FBG embedment in the targeted coils.

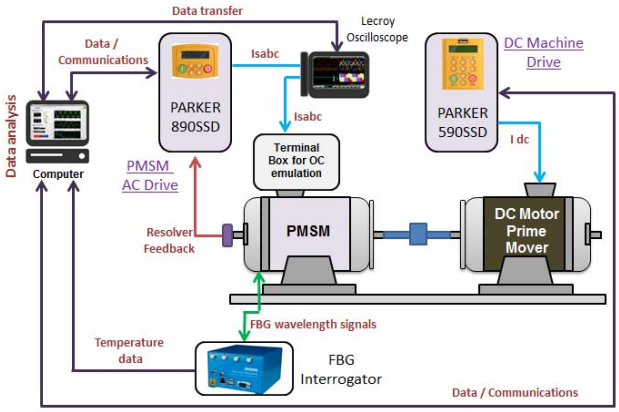

Fig. 9. Test rig setup.

by relevant standards [33] (i.e. one FBG per end-winding phase: FBG-EA, FBGB and FBG-EC, see Fig. 7b). This sensing distribution enables performance comparison between OC fault thermal signature monitored by FBGs in slot sections but also in standard end-winding thermal sensing positions as applied in most modern electric machinery using conventional TC and RTD sensors.

B. Test-Rig System

The performance of the proposed sensing scheme was examined in experiments on a laboratory test-rig whose configuration is shown in Fig. 9. The PMSM instrumented with FBGs was coupled to a 15.5 kW DC motor prime mover controlled via a Parker 590SSD drive. The PMSM was driven by a Parker 890SSD drive operating in Permanent Magnet Alternating Current (PMAC) vector control mode. The PMSM phase A current and voltage were monitored by LeCroy CP150 current and ADP300 voltage probes connected to a LeCroy 434 digital oscilloscope sampling at 5 kHz to record the data during the tests. The FBG sensors were illuminated using a broadband light source provided by a commercial multi-channel interrogator unit. The monitored FBG wavelengths were processed using Lab VIEW based SmartSoft software.

IV. Results and Discussion

This section reports the results of the experimental study undertaken to evaluate the application of the proposed in-situ thermal monitoring scheme on the inverter driven PMSM test-rig. Its efficacy for OC fault diagnosis in steady-state thermal conditions was first examined and verified, including a performance evaluation depending on sensing location. The diagnostic performance was then compared with the commonly proposed MCSA method to further illustrate the attained advantages. OC fault severities of 1, 2, 3 and 4 parallel strands OCs were practically examined. For each considered fault case, tests were performed at nominal speed, 1500 rpm, and at 50% and 100% of nominal load conditions. Tests were constrained to assessing a maximum of 4 strand OC fault in order to avoid permanent test machine damage.

A. Test Procedure Description

The test method applied for each examined fault case involved waiting for the thermal equilibrium to first be achieved to perform the following procedure: the healthy winding hot spot temperatures at thermal equilibrium were first monitored for 60 seconds. After this, an OC fault in one or more phase A strands was induced and maintained for a period of 60 seconds and thermal readings taken at a rate of 4 Hz. Finally, the fault was removed and thermal readings recorded during the cooling down period until the corresponding healthy winding thermal equilibrium has been reestablished. Phase A current rms value was also recorded, twice for each examined fault case: once in healthy condition and once in faulty condition. To practically emulate OC fault, the faulted strands were directly disconnected using a set of electrical switches during fault tests.

B. Induced OC Fault Thermal Signature Monitoring

The thermal measurements obtained in the tests are shown in Fig. 10 for 100% load operating conditions, and in Fig. 11 for 50% load operating conditions. To clearly illustrate the observed thermal changes, the recorded temperature rise with respect to healthy thermal steady-state is presented.

1) In-Situ Slot Section FBG Performance: In the case of 100% load operating conditions, a temperature rise of $\approx$1.75 °C was measured by FBG-SA at the lowest case of fault severity (1 strand OC) and $\approx$11.1 °C at the highest examined fault severity (4 strand OC). The FBG sensor embedded in the healthy phase C reports a very slight thermal rise due to the heat transfer between neighboring coils of phase A. In contrast, the FBG sensor in the other healthy phase, B, reports an insignificant thermal rise rate; this can be explained by the fact that the coils of this phase are located away from the fault induced thermal stress (refer to sensing positions in Fig. 7). At 50% load operating conditions, a temperature rise of $\approx$0.37 °C was measured by FBG-SA when a single strand is disconnected, and $\approx$2.6 °C at the highest severity. The in-situ measured temperature rise trends observed in healthy phases B and C are largely consistent with those recorded at 100% load conditions. More importantly, the OC fault thermal signature is seen to be clearly distinguishable in the faulty phase from the fault onset. The discrepancy between the in-situ hot spot temperature rise sensed values (Fig. 10) and those predicted by FEA thermal study (Table II) is because the FEA simulated fault condition temperatures are for thermal steady-state conditions, while in practical fault experiments the temperature was recorded only for a 60 seconds period for winding protection purpose, due to the potentially destructive

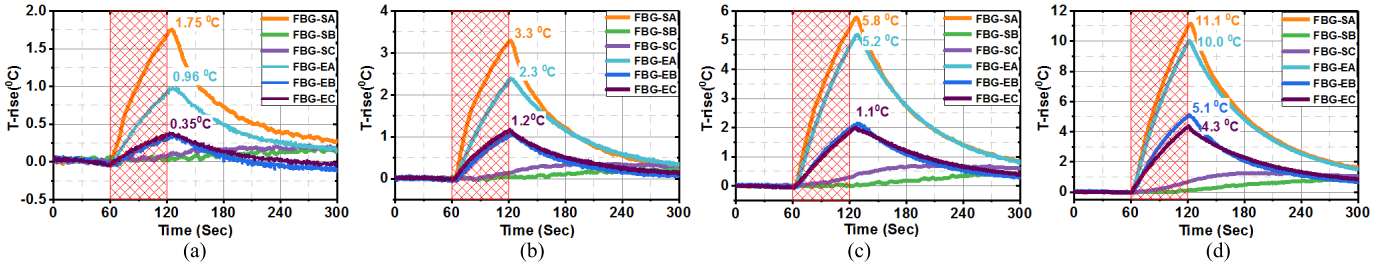

Fig. 10. Measured temperature rise profiles under OC fault condition at nominal speed and 100% load conditions; (a) 1 strand OC fault, (b) 2 strand OC fault, (c) 3 strand OC fault, and (d) 4 strand OC fault.

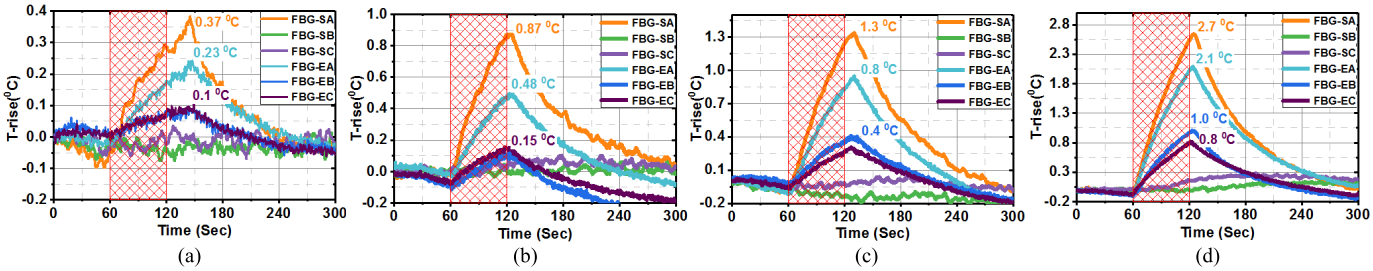

Fig. 11. Measured temperature rise profiles under OC fault condition at nominal speed and 50% load conditions; (a) 1 strand OC fault, (b) 2 strand OC fault, (c) 3 strand OC fault, and (d) 4 strand OC fault.

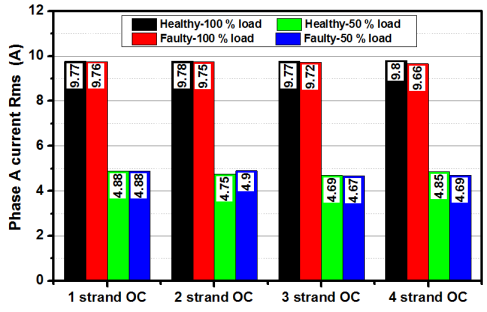

Fig. 12. Measured phase *A* current in PMSM.

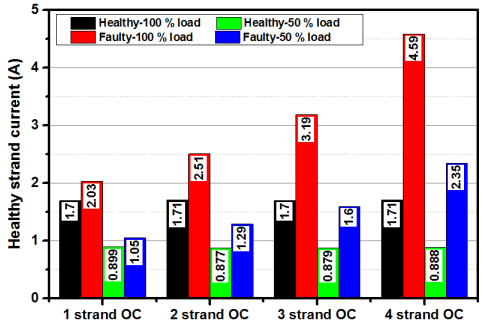

Fig. 13. Measured strand current in PMSM.

nature of the emulated fault if allowed to propagate towards fault thermal steady-state.

2) Performance Comparison With Standard Sensing Locations: The synchronously recorded thermal measurements by FBGs in the slot and end-winding sections in Figs. 10 and 11 show that FBGs located in slots exhibit higher sensitivity to fault induced thermal signature: these consistently report higher level of temperature rise and higher rate of temperature change compared to end-winding FBGs. In full load test conditions, the FBG-EA recorded the temperature rise of 0.96 °C, 2.3 °C, 5.2 °C and 10 °C for 1, 2, 3 and 4 OC test, respectively, constantly lower than readings provided by FBG-SA. The FBG-SA and FBG-EA reported readings differ by 45%, 30%, 10% and 9%, for 1, 2, 3 and 4 OC tests respectively, and are seen to particularly strongly contrast at incipient OC fault levels; this further highlights the diagnostic deficiency of in-situ thermal monitoring in end-winding locations in terms of timely detection of fault signature. As an illustration, in full load and 1 OC fault test, the maximum temperature rise level (0.96 °C) measured by FBG-EA was registered 30 seconds earlier by FBG-SA. Furthermore when FBG-SA registered the value of 0.96 °C, the FBG-EA measured temperature was a significantly lower 0.47 °C. Finally, the healthy phases' end-winding sensors (FBG-EB & FBG-EC) recorded higher temperature rise than their slot section sensors (FBG-SB & FBG-SC). This is a consequence of end-winding design nature that largely acts as a single thermal component averaging thermal readings, and in this case reporting a noticeable thermal increase in healthy end windings caused by the faulty phase that could complicate diagnosis; no such issues arise in in-slot FBG measurements.

The experimental data in Figs. 10–11 demonstrate the capability of the proposed in-situ thermal sensing and monitoring scheme for clear and effective recognition of OC fault localized thermal signature in PMSMs with stranded windings. The in-situ FBG sensor (FBG-SA) in the faulty phase is able to instantaneously measure the additional temperature rise due to current rebalancing in the faulted phase remaining strands during fault. The FBG embedded in the slot section shows higher sensitivity to OC fault induced thermal signature when

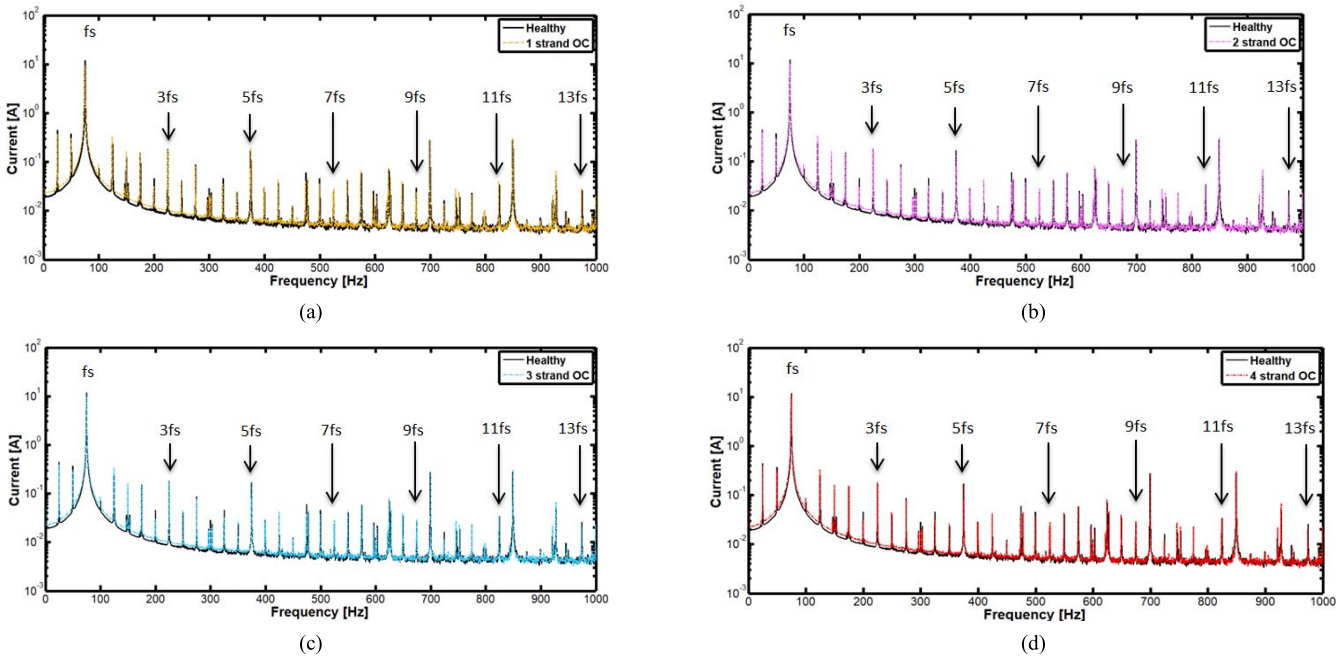

Fig. 14. Measured MCSA spectrum comparison under OC fault condition at nominal speed and 100% load conditions; (a) 1 strand OC fault, (b) 2 strand OC fault, (c) 3 strand OC fault, and (d) 4 strand OC fault.

compared to FBG end-winding sensor. This can enable faster fault recognition and ultimately provide more valuable time for the operator to react and mitigate undesirable fault effects.

C. Time Domain Current Monitoring

To enable further understanding of the diagnostic potential of in-situ thermal sensing and experimental results presented in Fig. 10 and Fig. 11, a comparison of the current flow in phase A with respect to the OC fault severity and load dependency was performed. Fig. 12 shows the measured healthy and faulted phase A current rms values for all examined loads and OC severities. The measurements show that there is no perceivable variation of the phase current magnitude due to OC fault thus confirming the electromagnetic FEA simulation study results in Fig. 2 and the associated discussion in section II.

To further illustrate this phenomenon, the current in one strand of phase A was additionally sensed and monitored during tests in healthy and faulty conditions and the results are shown in Fig. 13. As can be seen, during healthy operation, the phase current is distributed between the six parallel strands making up the phase winding; this current magnitude is load dependent (black and green bars). With an OC fault presence, the increase in strand current magnitude is clearly observable (red and blue bars). As the strand power loss (i.e. associated heat loss and resulting in-situ thermal excitation) is directly proportional to square of strand current the OC fault will invariably yield an increase in localized thermal conditions in the faulty phase, as shown by the thermal measurements in Fig 10 and 11. In reality, the measurements of parallel strand currents are not practically accessible to be used as a fault diagnostic feature; for example, for the examined motor this would require installation of additional 18 current sensors in the machine geometry which would impose prohibitive application constraints in field application. To the contrary a dedicated in-situ FBG thermal sensing system, such as that reported in this work can enable clear recognition of fault associated thermal effects and in addition provide enhanced information on the healthy motor thermal status. The presented current measurements further illustrate the importance of ensuring provision of an effective stranded winding PMSM OC fault diagnosis system: conventional phase current based PMSM protection systems will not react to this type of fault, since there is no significant change in the phase current to provide a trip warning for the protection system. This was observed on the commercial equipment used in the tests: the test motor was not tripped during fault experiments by the commercial protection system integrated in the utilized drive.

D. Motor Current Signature Analysis Performance Comparison

To further demonstrate the diagnostic potential of the proposed scheme for PMSM OC fault detection, this section presents the diagnostic signatures obtained from applying the conventionally accepted machine diagnostic technique of motor current signature analysis on the tested motor.

The PMSM phase A current sensed during tests was recorded and post-processed using the MATLAB FFT routine with a 2^{15} data point resolution to extract and examine its spectrum. For illustration purposes, Fig. 14 shows the results of the measured current spectra at 100% of load and different fault severities. The measured spectra are seen to contain the fs frequency component and its odd harmonics reflecting the generator operation FEA simulations results discussed in section II.A. The observed components originate from the

TABLE III
HARMONIC COMPONENTS VARIATION

	Healthy	1 strand	2 strands	3 strands	4 strands
Harmonic Component	% Fundamental	% Fundamental	% Fundamental	% Fundamental	% Fundamental
3	1.54	1.88	1.81	1.80	1.81
5	1.42	1.99	1.77	1.67	1.77
7	0.21	0.29	0.28	0.29	0.29
9	0.25	0.26	0.30	0.29	0.30
11	0.29	0.41	0.34	0.34	0.34
13	0.22	0.19	0.21	0.21	0.21

spatial distribution of the air-gap flux density produced by the rotor permanent magnets; the rich additional spectral content in the measured spectra results from the nature of the inverter driven vector controlled PMSM operation examined [34]. In terms of reliable fault signature recognition, the harmonic magnitude changes measured in the test PMSM current spectrum do not present a clear trend with respect to OC fault severity, and the application of their observed modest variation with fault for OC fault diagnosis would be challenging and inconclusive as shown in Table III summarizing the measured harmonic magnitudes. In contrast, the in-situ monitored thermal signature presented in Figs. 4–5 enables unambiguous diagnosis of each of the analyzed strand OC faults scenarios.

V. CONCLUSION

This study researches the application of in-situ FBG sensing for thermal hot spot monitoring in stranded winding permanent magnet synchronous machines with a view to enabling improved open circuit winding fault detection. FEA thermal and electric models of the examined commercial machine design are developed and utilized to show that the optimal diagnostic indicator of open circuit fault is the winding thermal hot spot temperature.

To enable the required hot spot temperature monitoring a thermal FBG sensor design is used that allows winding embedded in-situ sensing in the coils' slot section cross sectional center point, which in combination with inherent FBG sensing feature of full EMI immunity provides unparalleled operational features for this application. A commercial inverter driven permanent magnet motor was instrumented with FBG thermal sensors and a range of experiments undertaken in healthy and varying degrees of winding open circuit fault conditions. It is shown that the proposed FBG in-situ sensing scheme enables unambiguous fault diagnosis and severity trending in practical operation conditions.

A diagnostic performance comparison of the reported FBG sensor underpinned scheme with conventional electric signal signature analysis techniques is also reported, showing that the use of FBG sensors for condition monitoring and diagnostic purposes in stranded winding permanent magnet synchronous machines can provide attractive advantages in attaining reliable fault detection and recognition of its severity.

REFERENCES

[1] J.-C. Urresty, J.-R. Riba, and L. Romeral, "A back-EMF based method to detect magnet failures in PMSMs," *IEEE Trans. Magn.*, vol. 49, no. 1, pp. 591–598, Jan. 2013.

[2] S. Choi *et al.*, "Fault diagnosis techniques for permanent magnet AC machine and drives—A review of current state of the art," *IEEE Trans. Transp. Electrific.*, vol. 4, no. 2, pp. 444–463, Jun. 2018.

[3] B. Akin, S. Choi, U. Orguner, and H. A. Toliyat, "A simple real-time fault signature monitoring tool for motor-drive-embedded fault diagnosis systems," *IEEE Trans. Ind. Electron.*, vol. 58, no. 5, pp. 1990–2001, May 2011.

[4] W. Le Roux, R. G. Harley, and T. G. Habetler, "Detecting rotor faults in low power permanent magnet synchronous machines," *IEEE Trans. Power Electron.*, vol. 22, no. 1, pp. 322–328, Jan. 2007.

[5] G. C. Stone, "Condition monitoring and diagnostics of motor and stator windings—A review," *IEEE Trans. Dielectr. Electr. Insul.*, vol. 20, no. 6, pp. 2073–2080, Dec. 2013.

[6] T.-J. Kang, J. Hong, S. B. Lee, Y.-W. Yoon, D.-H. Hwang, and D. Kang, "The influence of the rotor on surge pd testing of low voltage AC motor stator windings," *IEEE Trans. Dielectr. Electr. Insul.*, vol. 20, no. 3, pp. 762–769, Jun. 2013.

[7] J. Li *et al.*, "Research on stator winding open circuit faults of permanent magnet wind turbine," in *Proc. 20th Int. Conf. Elect. Mach. Syst. (ICEMS)*, Sydney, NSW, Australia, Aug. 2017, pp. 1–5.

[8] M. Malekpour, B. T. Phung, and E. Ambikairajah, "Online technique for insulation assessment of induction motor stator windings under different load conditions," *IEEE Trans. Dielectr. Electr. Insul.*, vol. 24, no. 1, pp. 349–358, Feb. 2017.

[9] A. Boglietti *et al.*, "Electrical machine topologies: Hottest topics in the electrical machine research community," *IEEE Ind. Electron. Mag.*, vol. 8, no. 2, pp. 18–30, Jun. 2014.

[10] X. Xu, Q. Han, and F. Chu, "Review of electromagnetic vibration in electrical machines," *Energies*, vol. 11, no. 7, p. 1779, 2018.

[11] J. Hang, S. Ding, J. Zhang, M. Cheng, and Q. Wang, "Open-phase fault detection in delta-connected PMSM drive systems," *IEEE Trans. Power Electron.*, vol. 33, no. 8, pp. 6456–6460, Aug. 2018.

[12] J. Apsley and S. Williamson, "Analysis of multiphase induction machines with winding faults," *IEEE Trans. Ind. Appl.*, vol. 42, no. 2, pp. 465–472, Mar./Apr. 2006.

[13] J. Faiz and E. Mazaheri-Tehrani, "Demagnetization modeling and fault diagnosing techniques in permanent magnet machines under stationary and nonstationary conditions: An overview," *IEEE Trans. Ind. Appl.*, vol. 53, no. 3, pp. 2772–2785, May/Jun. 2017.

[14] S. Nandi, H. A. Toliyat, and X. Li, "Condition monitoring and fault diagnosis of electrical motors—A review," *IEEE Trans. Energy Convers.*, vol. 20, no. 4, pp. 719–729, Dec. 2005.

[15] N. Leboeuf, T. Boileau, B. Nahid-Mobarakeh, N. Takorabet, F. Meibody-Tabar, and G. Clerc, "Estimating permanent-magnet motor parameters under inter-turn fault conditions," *IEEE Trans. Magn.*, vol. 48, no. 2, pp. 963–966, Feb. 2012.

[16] L. Romeral, J. C. Urresty, J.-R. R. Ruiz, and A. G. Espinosa, "Modeling of surface-mounted permanent magnet synchronous motors with stator winding interturn faults," *IEEE Trans. Ind. Electron.*, vol. 58, no. 5, pp. 1576–1585, May 2011.

[17] N. Leboeuf, T. Boileau, B. Nahid-Mobarakeh, N. Takorabet, F. Meibody-Tabar, and G. Clerc, "Inductance calculations in permanent-magnet motors under fault conditions," *IEEE Trans. Magn.*, vol. 48, no. 10, pp. 2605–2616, Oct. 2012.

[18] K. Liu and Z. Q. Zhu, "Position-offset-based parameter estimation using the adaline NN for condition monitoring of permanent-magnet synchronous machines," *IEEE Trans. Ind. Electron.*, vol. 62, no. 4, pp. 2372–2383, Apr. 2014.

[19] R. M. Tallam *et al.*, "A survey of methods for detection of stator-related faults in induction machines," *IEEE Trans. Ind. Appl.*, vol. 43, no. 4, pp. 920–933, Jul./Aug. 2007.

[20] S. Grubic, J. M. Aller, B. Lu, and T. G. Habetler, "A survey on testing and monitoring methods for stator insulation systems of low-voltage induction machines focusing on turn insulation problems," *IEEE Trans. Ind. Electron.*, vol. 55, no. 12, pp. 4127–4136, Dec. 2008.

[21] G. N. Surya, Z. J. Khan, M. S. Ballal, and H. M. Suryawanshi, "A simplified frequency-domain detection of stator turn fault in squirrel-cage induction motors using an observer coil technique," *IEEE Trans. Ind. Electron.*, vol. 64, no. 2, pp. 1495–1506, Feb. 2017.

[22] S. D. Wilson, G. W. Jewell, and P. G. Stewart, "Resistance estimation for temperature determination in PMSMs through signal injection," in *Proc. IEEE Int. Conf. Electr. Mach. Drives*, San Antonio, TX, USA, May 2005, pp. 735–740.

[23] G. Singh, T. C. A. Kumar, and V. N. A. Naikan, "Induction motor inter turn fault detection using infrared thermographic analysis," *Infr. Phys. Technol.*, vol. 77, pp. 277–282, Jul. 2016.

[24] A. Mohammed and S. Djurović, "Stator winding internal thermal monitoring and analysis using *in situ* FBG sensing technology," *IEEE Trans. Energy Convers.*, vol. 33, no. 3, pp. 1508–1518, Sep. 2018.
[25] K. M. Sousa, I. B. V. da Costa, E. S. Maciel, J. E. Rocha, C. Martelli, and J. C. C. da Silva, "Broken bar fault detection in induction motor by using optical fiber strain sensors," *IEEE Sensors J.*, vol. 17, no. 12, pp. 3669–3676, Jun. 2017.
[26] J. M. Corres, J. Bravo, F. J. Arregui, and I. R. Matias, "Unbalance and harmonics detection in induction motors using an optical fiber sensor," *IEEE Sensors J.*, vol. 6, no. 3, pp. 605–612, Jun. 2006.
[27] K. M. Sousa, U. J. Dreyer, C. Martelli, and J. C. C. da Silva, "Dynamic eccentricity induced in induction motor detected by optical fiber Bragg grating strain sensors," *IEEE Sensors J.*, vol. 16, no. 12, pp. 4786–4792, Jun. 2016.
[28] A. Mohammed and S. Djurović, "FBG thermal sensing features for hot spot monitoring in random wound electric machine coils," *IEEE Sensors J.*, vol. 17, no. 10, pp. 3058–3067, May 2017.
[29] A. Mohammed and S. Djurović, "A study of distributed embedded thermal monitoring in electric coils based on FBG sensor multiplexing," *Microprocessors Microsyst.*, vol. 62, pp. 102–109, Oct. 2018.
[30] D. Casadei, F. Filippetti, C. Rossi, and A. Stefani, "Magnets faults characterization for permanent magnet synchronous motors," in *Proc. IEEE Int. Symp. Diag. Electr. Mach., Power Electron. Drives*, Cargese, France, Aug./Sep. 2009, pp. 1–6.
[31] I. J. Melecio, S. Djurović, and N. Schofield, "An FEA model study of spectral signature patterns of PM demagnetisation faults in synchronous PM machines," in *Proc. 9th Int. Conf. Power Electron., Machines and Drives (PEMD)*, Liverpool, U.K., Apr. 2018, pp. 1–6.
[32] Y.-J. Rao, "In-fibre Bragg grating sensors," *Meas. Sci. Technol.*, vol. 8, no. 4, p. 355, 1997.
[33] *Rotating Electrical Machines—Part 1: Rating and Performance*, Standard IEC 60034-1:2010, 2010.
[34] J. O. Estima and A. J. M. Cardoso, "The occurrence of faults in permanent magnet synchronous motor drives and its effects on the power supply quality," *Renew. Energy Power Qual. J.*, vol. 1, no. 6, pp. 312–317, Mar. 2008.

Anees Mohammed received the M.Sc. degree in electrical power engineering from The University of Newcastle, U.K., in 2010. He is currently pursuing the Ph.D. degree in electrical and electronic engineering with The University of Manchester, U.K. He spent four years as an Assistant Lecturer with Benghazi University, Libya. His research interests are in electric machines, drives, and condition monitoring.

Juan I. Melecio received the B.S. degree in mechatronics engineering and the M.Sc. degree in energy engineering from Tecnológico de Monterrey. He is currently pursuing the Ph.D. degree in electrical and electronic engineering with The University of Manchester, U.K. He spent five years with Schneider Electric, Monterrey, Mexico, and Cedar Rapids, IA, USA. His current research interests include finite-element analysis, electrical machines, drives, and condition monitoring.

Siniša Djurović (M'09) received the Dipl.Ing. degree in electrical engineering from the University of Montenegro in 2002 and the Ph.D. degree from The University of Manchester in 2007.

He is currently a Senior Lecturer with the Power Conversion Group, The University of Manchester. His research interests are in the areas of operation, design, monitoring, and diagnostics of electric machines and drives.